Dalton Transactions

Accepted Manuscript

This is an *Accepted Manuscript*, which has been through the Royal Society of Chemistry peer review process and has been accepted for publication.

Accepted Manuscripts are published online shortly after acceptance, before technical editing, formatting and proof reading. Using this free service, authors can make their results available to the community, in citable form, before we publish the edited article. We will replace this *Accepted Manuscript* with the edited and formatted *Advance Article* as soon as it is available.

You can find more information about *Accepted Manuscripts* in the Information for Authors.

ROYAL SOCIETY OF CHEMISTRY

www.rsc.org/dalton

Journal of Materials Chemistry RSCPublishing

ARTICLE

α-$Na_2Ni_2Fe(PO_4)_3$: a Dual Positive/Negative Electrode Material for Sodium Ion Batteries

Cite this: DOI: 10.1039/x0xx00000x

R. Essehli,[a,*] I. Belharouak,[a,*] H. Ben Yahia,[a,*] R. Chamoun,[a] B. Orayech,[b] B. El Bali,[c] K. Bouziane,[d] X. Zhou,[e] and Z. Zhen[e]

Received 00th January 2012,
Accepted 00th January 2012

DOI: 10.1039/x0xx00000x

www.rsc.org/

The new orthophosphate α-$Na_2Ni_2Fe(PO_4)_3$ was synthesized using a solid state reaction route, and its crystal structure was determined from powder X-ray diffraction data. The physical properties of α-$Na_2Ni_2Fe(PO_4)_3$ were studied by magnetic and electrochemical measurements and by Mössbauer and Raman spectroscopies. α-$Na_2Ni_2Fe(PO_4)_3$ crystallizes according to a stuffed α-$CrPO_4$-type structure with thespace group *Imma* and the cell parameters a = 10.42821(12), b = 13.19862(15), c = 6.47634(8) Å, and Z = 4. The structure consists of a 3D-framework of octahedra and tetrahedra sharing corners and/or edges with channels along [100] and [010], in which the sodium atoms are located. The ^{57}Fe Mössbauer spectrum indicates that the Fe^{3+} cation is distributed over two crystallographic sites implying the presence of a Ni^{2+}/Fe^{3+}statistical disorder. The magnetic susceptibility follows the Curie-Weiss behavior above 100 K with θ = -114.3 K indicating the occurrence of predominant antiferromagnetic interactions. The electrochemical tests indicate that during the first discharge to 1 V *vs.* Na^+/Na in a sodium cell, one Na^+ ion could be inserted into α-$Na_2Ni_2Fe(PO_4)_3$ structure. This has led to the formation of a new phase $Na_3Ni_2Fe(PO_4)_3$ which was found to be promising as a positive electrode material for sodium batteries. When α-$Na_2Ni_2Fe(PO_4)_3$ is further discharge to 0.03 V, it delivers a capacity of 960 mAh/g. This corresponds to the intercalation of more than seven sodium atoms per formula unit which is an indication of a conversion-type behaviour with the formation of metallic Fe and Ni. When cycled in the voltage range 0.03-3 V *vs.* Na^+/Na, at 20 ^oC, under the current rates of 50, 100, 200, and 400 mA/g, reversible capacities of 238, 196, 153, and 115 mAh/g, were obtained, respectively.

1. Introduction

The Lithium ion batteries (LiIBs) have attracted, during the last four decades, the attention of researchers from different fields, due to their use in practical applications such as Laptops, cellphones, toys, etc. This attention has been renewed recently, since LiIBs are promising for large scale energy storage applications such as electric vehicles and grid storage applications. Indeed, the olivine $LiFePO_4$ (theoretical capacity = 170 mAh/g), which is used in the new generation of LiIBs, is a particularly promising example due to its advantages of being environmentally benign and safe. [1,2] However, with lithium based cathode materials, there are concerns with regard to the abundance of lithium in the earth crust. Recent reports have pointed out sodium ion batteries (NaIBs), as energy storage systems, worthy of intensive investigation for large battery applications, since the sodium reserves are easily accessible.[3, 4]

It remains a practical challenge to find electrochemical couples (cathodes and anodes) that are suitable in terms of capacity and cycle life for NaIBs. During the last twenty years, there have been few attempts to discover new sodium and iron-based polyanionic compounds whose crystal structures and iron neighborhood give raise to different Fe^{3+}/Fe^{2+} redox voltages. Among these materials, the phosphates $NaMnFe_2(PO_4)_3$, $[Na_{1-x}Li_x]MnFe_2(PO_4)_3$, $Na_3Fe_3(PO_4)_4$, $Na_3Fe_2(PO_4)_3$, $Na_2Fe_{3-x}Mn_x(PO_4)_3$, $NaFe(PO_4)$, $Na_3Fe(PO_4)(CO_3)$, $Na_2Fe(P_2O_7)$, $Na_4Fe_3(PO_4)_2(P_2O_7)$, or Na_2FePO_4F have been tested as positive or negative electrodes for NaIBs.[5-12] These compounds crystallize with different type of structures. The alluaudite-type structure with the general formula $AA'BB'_2(PO_4)_3$ (A and A' = Li, Na, □; B is a large six coordinated cation such as Li, Na, Mn-Ni; B' is a small six coordinated cation such as Mn-Ni) has been intensively studied as electrode materials for LiIBs and/or NaIBs.[4-7] Hatert et *al*. reported that beside the conventional atomic positions of A and A' in the tunnels, there exists additional vacancies in which Li^+ and/or Na^+ might be inserted.[13] The presence of Fe^{3+} or Mn^{3+} in the structure is therefore required, since the intercalation of Li^+ or Na^+ has to be accompanied by the reduction of the trivalent transition

metal. Following this idea, we prepared the $Na_2Ni_2Fe(PO_4)_3$ composition as positive and negative electrode material for NaIBs. Surprisingly, the latter compound exhibited two polymorphs. The high-temperature form (β) is isostructural to the alluaudite-type structure,[14] whereas the low temperature form (α) is considered as a stuffed α-$CrPO_4$-type structure.

In the present work we synthesized a new compound α-$Na_2Ni_2Fe(PO_4)_3$, solved the crystal structure using powder X-ray diffraction data (PXRD), and characterized its electrochemical and magnetic properties. We also characterized α-$Na_2Ni_2Fe(PO_4)_3$ by Mössbauer and Raman spectroscopy.

2. Experimental Section

2.1. Synthesis

The title compound α-$Na_2Ni_2Fe(PO_4)_3$ was prepared by solid state reaction, from stoichiometric mixtures of Na_2CO_3 (Aldrich, 99.5 %), $Ni(NO_3)_2$•$6H_2O$ (Merck, 99.9 %), $Fe(NO_3)_3$•$9H_2O$ (Merck, 99 %), and $NH_4H_2PO_4$ (Aldrich, 99.99 %). The starting materials were ground in an agate mortar, put into platinum crucible and heated at 200 °C for 6h and at 500 °C for 24 h in air in order to release H_2O, NH_3, and CO_2. The resulting powder was then ground and heated at 850 °C for 48 h. The progress of the reactions was followed by PXRD and the powder sample was pure. It is worth mentioning that a thermal treatment above 850 °C would induce an irreversible phase transition from α- to β-$Na_2Ni_2Fe(PO_4)_3$.[14]

2.2. Powder X-Ray diffraction measurements

To ensure the purity of α-$Na_2Ni_2Fe(PO_4)_3$ powder, high precision PXRD measurements were performed. The data were collected at room temperature over the 2θ angle range of $10° \leq 2\theta \leq 110°$ with a step size of 0.01 ° using a Panalytical diffractometer operating with Cu*K*α radiations. Full pattern matching refinement was performed with the Jana2006 program package.[15] The background was estimated by a Legendre function, and the peak shapes were described by a pseudo-Voigt function. The refinement of peak asymmetry was performed using four Berar-Baldinozzi parameters. Evaluation of these data revealed the refined cell parameters listed in Table 1.

2.3. Raman spectroscopy

Raman spectra were measured in a back scattering arrangement, at room temperature and ambient pressure, by using a high-throughput holographic imaging spectrograph with volume transmission grating, holographic notch filter and thermoelectrically cooled CCD detector (Physics Spectra). The spectrometer was regularly calibrated by using the neon lines. Ti^{3+}–sapphire laser pumped by an argon ion laser was tuned at 700 nm. The acquisition time was 60 s.

2.4. Mössbauer spectroscopy

The ^{57}Fe Mössbauer spectra of α-$Na_2Ni_2Fe(PO_4)_3$ were collected in transmission geometry with a constant acceleration spectrometer using ^{57}Co γ-ray source. The velocity calibration was done at room temperature with a high purity α-Fe absorber. The experimental data were fitted to two symmetric doublets consisting of Lorentzian lines by using the least-squares method. The isomer shift (IS) values are given relative to that of α-Fe at room temperature.

Table 1. Crystallographic and structure refinements data for α-$Na_2Ni_2Fe(PO_4)_3$.

Rietveld Refinement	
Crystal data	
Chemical formula	α-$Na_2Ni_2FeP_3O_{12}$
M_r	504.1
Crystal system	Orthorhombic
Space group	*Imma* (No 74)
Temperature (K)	300
a (Å)	10.42821 (12)
b (Å)	13.19862 (15)
c (Å)	6.47634 (8)
V (Å^3)	891.39 (2)
Z	4
Data collection	
Diffractometer	Panalytical
Radiation type	$Cu_{\alpha1,\alpha2}$
$2\theta_{min}$, $2\theta_{step}$, $2\theta_{max}$ values (°)	10, 0.01, 100
Refinement	
R_p	0.018
R_{wp}	0.023
R_{exp}	0.020
$R(F)$	0.068
R_{Bragg}	0.087
goodness of fit χ^2	1.322
No. of data points	9000
No. of parameters	42
Profile function	Pseudo-Voigt
Background	Chebyshev function with15 terms

2.5. Magnetic characterizations

Magnetic susceptibility measurements of α-$Na_2Ni_2Fe(PO_4)_3$ were carried out with a DMS 1660 vibrating sample magnetometer (VSM). The susceptibility was recorded in the zero field cooled (ZFC) and field cooled (FC) modes, in the temperature range 2 – 350 K, with an applied external field of 100 Oe.

2.6. Electrochemical cycling

All electrochemical tests were made on half-cells in a thermostatic bath maintained at 25°C. The electrodes were made a from mixture of α-$Na_2Ni_2Fe(PO_4)_3$ powder (active material), super-P carbon (conductive additive), and PVDF (binder) in a weight ratio of 80:15:5. This mixture was compressed into sheets, cut into 8-mm-diameter discs, loaded onto Cu foil, and dried at 100°C overnight. α-$Na_2Ni_2Fe(PO_4)_3$/$NaPF_6$-EC-DMC/Na coin-type cells (CR2032) were assembled in an argon-filled glove box. The room-temperature electrochemical performances were evaluated by galvanostatic charge/discharge cycling at different current rates, in the voltage range 0.03–3.0 V *vs.* Na^+/Na.

The new material $Na_3Ni_2Fe(PO_4)_3$ was obtained by discharging the α-$Na_2Ni_2Fe(PO_4)_3$/$NaPF_6$-EC-DMC/Na coin-type cell down to 1V. The $Na_3Ni_2Fe(PO_4)_3$ electrode was then washed several times with EC, dried, and used as positive electrode. The galvanostatic charge/discharge cycling were performed at a rate of 5 mA/g in the voltage range 1.8–4.5 V *vs.* Na^+/Na.

Table 2. Atom positions and isotopic displacement parameters for α-$Na_2Ni_2Fe(PO_4)_3$ from X-ray powder diffraction data at 300K.

Atom	Wyck.	Occ.	*x*	*y*	*z*	U_{iso} (Å^2)
Na1	4*e*		0	3/4	0.6119(14)	0.094(3)
Na2	4*b*		0	1/2	1/2	0.094(3)
Ni1/Fe1	8*g*	0.75/0.25	1/4	0.63617(17)	1/4	0.0035(6)
Ni2/Fe2	4*a*	0.5/0.5	1/2	1/2	1/2	0.0035(6)
P1	8*g*		1/4	0.4288(3)	1/4	0.0070(12)
P2	4*e*		0	3/4	0.0831(8)	0.0070(12)
O1	16*j*		0.2881(4)	0.3660(4)	0.0661(6)	0.0018(11)
O2	16*j*		0.1403(4)	0.5066(3)	0.2117(8)	0.0018(11)
O3	8*h*		0	0.6538(6)	0.9525(10)	0.0018(11)
O4	8*i*		0.1202(6)	3/4	0.2280(13)	0.0018(11)

3. RESULTS AND DISCUSSION

3.1. Structure refinement

The crystal structure of α-$Na_2Ni_2Fe(PO_4)_3$ was solved using the crystal structure of Na□$V_3(PO_4)_3$ as starting model.[16] The cell parameters could be determined with dicvol and treor programs.[17, 18] The Rietveld analysis of the powder XRD data collected at 300 K led to the reliability factors [*R*p = 2.50%, *wR*p = 3.43%, R_B = 32% (χ^2 = 1.69)]. The use of difference-Fourier synthesis allowed us to localize the remaining sodium atom position. Consequently, the reliability factors decreased significantly [*R*p = 1.83%, *wR*p = 2.32%, R_B = 7.92% (χ^2 = 1.14)]. Since, few atomic displacement parameter (ADP) tensors displayed negative values; atoms of same nature have been restricted to have same ADPs. This led to the reliability factors listed in Table 1. The final atomic positions are given in Table 2. Fig. 1 shows a good agreement between the experimental and calculated patterns. One should mention that the nickel and iron atoms are statistically disordered over the two crystallographic sites (4*a*) and (8*g*), the Ni/Fe ratios have been fixed in agreement with the Mössbauer results (see Mössbauer section). The sodium atoms displayed large ADPs and the refinement of their occupancies did not show any significant deviation from the standard values. Therefore, the large ADPs values have been attributed to the high mobility of the sodium atoms.

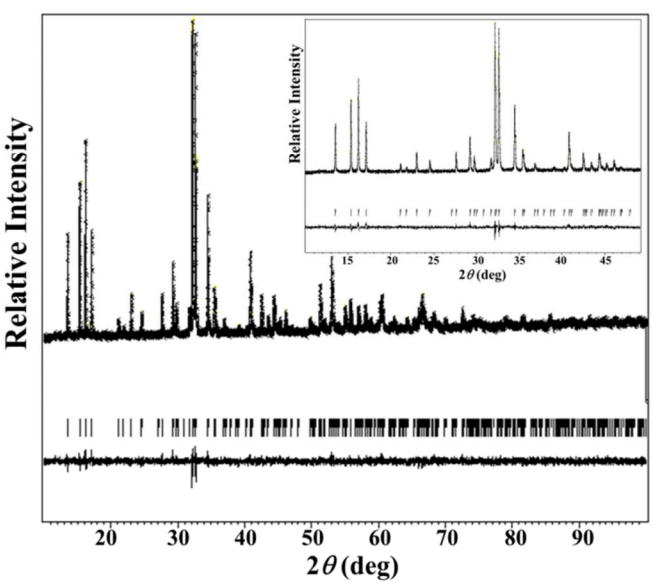

Fig. 1. Final observed, calculated and difference plots for XRPD (Cu-K_α radiation) refinement of α-$Na_2Ni_2Fe(PO_4)_3$. The inset corresponds to a zoom of the 2*θ* = 10 to 50 ° area.

3.2 Crystal Structure

α-$Na_2Ni_2Fe(PO_4)_3$ is isostructural to Na□$V_3(PO_4)_3$ and Sr□$Fe_3(PO_4)_3$ (□: vacancy) which crystallise with the a stuffed α-$CrPO_4$ type structure.[16-20] The structure consists of [Fe1/Ni1$_2$O$_{10}$] dimer units (edge-sharing octahedra) sharing corners with the [Fe2/Ni2O$_6$] octahedra (Fig. S1). These octahedra, containing statistically disordered Ni^{2+} and Fe^{3+}, share corners and edges with the PO_4 tetrahedra, thus giving rise to a three-dimensional framework with channels along [100] and [010], in which the sodium atoms are located (Figs. 2a, 2b). Interatomic distances and bond valence sums (BVSs) [21, 22] based on XRPD data are listed in Table 3.

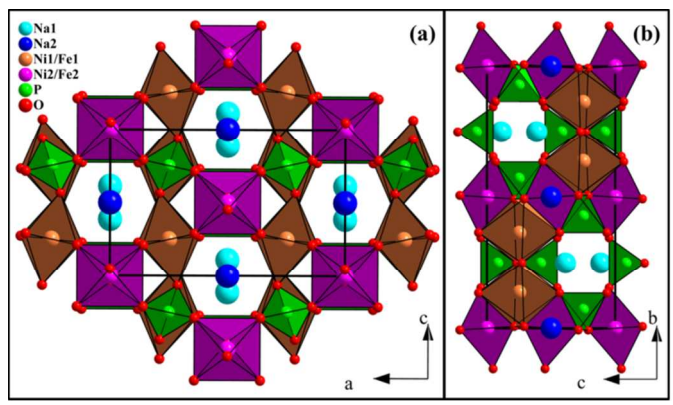

Fig. 2. Projection Views of the structure of α-$Na_2Ni_2Fe(PO_4)_3$ along the *b* axis (a), and the *a* axis (b).

In the [(Ni2/Fe2)O$_6$] octahedra the d(Ni2/Fe2-O) distances range from 2.007 to 2.054Å with an average distance of 2.0227 Å, whereas in the [(Ni1/Fe1)O$_6$] octahedra, the $d_{Ni1/Fe1-O}$ distances range from 2.027 to 2.086 Å with an average value of 2.0617 Å. Such Ni^{2+}/Fe^{3+} coordination and distances values have been also reported in $Ba_2FeNi[PO_4]_3$, in which average distances are 2.048 and 2.063 Å.[23]

The [P1O$_4$] tetrahedron is more distorted than [P2O$_4$] due to the presence of two short d_{P1-O1} distances of 1.505 Å which are close to the values found in $NaMnFe_2(PO_4)_3$.[5] The average d_{P-O} distances of 1.531 and 1.566 Å for P1 and P2, respectively, are consistent with the value of 1.55 Å estimated from the effective ionic radii of the four-coordinated P^{5+} and O^{2-}.[24] The BVSs of 5.06 and 4.86 are in agreement with the expected value of +5 for P^{5+}.

The $Na1^+$ and $Na2^+$ ions are bonded to eight oxygen atoms belonging to six and four different FeO_6 octahedra, respectively (Figs. 3a, 3b). The d_{Na1-O} and d_{Na2-O} distances range from 2.545 Å to 2.784 Å and from 2.374 Å to 2.863 Å with the average values of 2.685 Å and 2.619 Å, respectively. The BVS values of 0.760 and 1.083 respectively for Na1 and Na2, indicate that

Na1 is under bonded. Such Na coordinations have been also observed in alluaudite polymorph β-$Na_2Ni_2Fe(PO_4)_3$ (Figs. 4c, 4d).[14] This is very surprising since the α– and β-$Na_2Ni_2Fe(PO_4)_3$ polymorphs crystallize with significantly different structures (Figs.2a, 4a). Indeed, in β-$Na_2Ni_2Fe(PO_4)_3$ the octahedra share edges and form isolated infinite chains (Fig. 4b), whereas in α-$Na_2Ni_2Fe(PO_4)_3$, the octahedra share edges and corners and form a 3D-framework (Fig. S1). Furthermore, based on group-subgroup transformations, there is no obvious structural relationship between both polymorphs.

Table 3. Interatomic distances (in Å) and bond valences (B.V.) for α-$Na_2Ni_2Fe(PO_4)_3$. Average distances are given in brackets.

	Distance (Å)
Na1-O3 (×2)	2.545(10)
Na1-O1 (×4)	2.705(4)
Na1-O4 (×2)	2.784(11)
	<2.685>
	[a] 0.760 [8]
Na2-O2 (×4)	2.374(5)
Na2-O1 (×4)	2.863(4)
	<2.619>
	[a] 1.083 [8]
Ni1/Fe1-O4 (×2)	2.027(5)
Ni1/Fe1-O2 (×2)	2.072(5)
Ni1/Fe1-O1 (×2)	2.086(4)
	<2.0617>
	[a] 1.999/2.655 [6]
Ni2/Fe2-O2 (×4)	2.007(5)
Ni2/Fe2-O3 (×2)	2.054(7)
	<2.0227>
	[a] 2.218/2.946 [6]
P1-O1 (×2)	1.505(5)
P1-O2 (×2)	1.557(5)
	<1.531>
	[a] 5.060 [4]
P2-O3 (×2)	1.525(8)
P2-O4 (×2)	1.566(8)
	<1.5455>
	[a] 4.860 [4]

[a] bond valence sum, B.V. = $e^{(r0-r)/b}$ with the following parameters: b = 0.37, r_0 (Na^I–O) = 1.803, r_0 (Ni^{II}–O) = 1.654, r_0 (Fe^{III}–O) = 1.759, and r_0 (P^V–O) = 1.617 Å.[21, 22]

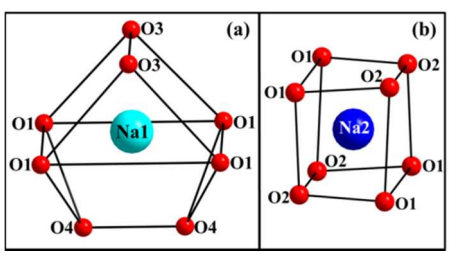

Fig. 3. Coordinations of the sodium atoms in α-$Na_2Ni_2Fe(PO_4)_3$.

3.3. Raman spectroscopy

The Raman spectrum of $Na_2Ni_2Fe(PO_4)_3$, measured in the range 1800-100 cm^{-1}, is depicted on Fig. S2. Its vibrational modes are due to PO_4 tetrahedra (internal and external modes) and to lattice modes of the octahedral coordinated transition metal atoms. The PO_4 unit gives vibrational modes that are characterized by symmetric ν_s (P-O), ν_d (P-O) (ν_1 and ν_3) and δ_d (O-P-O) bending (ν_2/ν_4). These modes are observed in the frequency ranges 1275-1000 cm^{-1} (ν_3), 1000-900 cm^{-1} (ν_1), 670-540 cm^{-1} (ν_4), and 460–425 cm^{-1} (ν_2). The PO_4 external modes corresponding to vibrational and translational motions of these groups are generally observed below 300 cm^{-1}.[14]

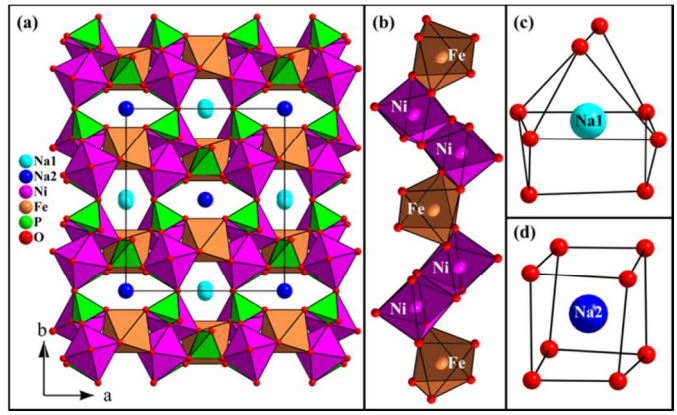

Fig. 4. Projections of the structure of β-$Na_2Ni_2Fe(PO_4)_3$ along the c axis (a), view of the infinite chains of edge-sharing octahedra (b), and surrounding of the sodium atoms (c, d).

3.4. ^{57}Fe Mössbauer spectroscopy

The ^{57}Fe Mössbauer spectrum of α-$Na_2Ni_2Fe(PO_4)_3$, measured at room temperature, is given in Fig. 5. In order to explain the experimental spectrum, it was necessary to consider two distributions corresponding to two trivalent iron atoms in octahedral environments. The characteristic parameters deduced from this refinement, the isomeric shift (δ), the full width at half maximum (Γ), and quadruple splitting (Δ), are given in Table 4.

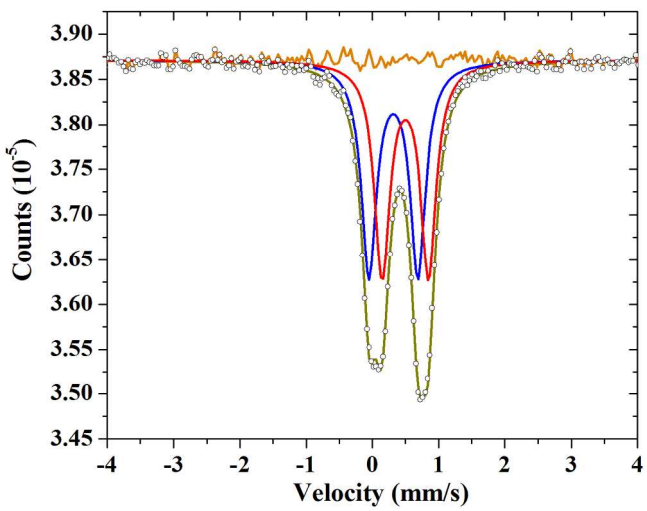

Fig. 5. ^{57}Fe Mössbauer experimental and fitted spectra of α-$Na_2Ni_2Fe(PO_4)_3$ collected at room temperature.The corresponding fitted parameters are given in Table 4.

Table 4. Fitted ^{57}Fe Mössbauer parameters obtained for α-$Na_2Ni_2Fe(PO_4)_3$ phase (δ = isomeric shift, Γ = full width at half maximum, and Δ = quadripole splitting).

Dis	δ /mm s^{-1}	Γ / mm s^{-1}	Δ/mm s^{-1}	%	Site
1	0.42 (1)	0.28 (1)	0.55 (2)	52 (2)	Fe^{3+} [O_h]
2	0.40 (1)	0.28 (1)	0.91 (2)	48 (2)	Fe^{3+} [O_h]

The spectrum exhibits two doublets with isomeric shifts of + 0.40(1) and + 0.42(1) mm s^{-1} which are typical values obtained for Fe^{3+} in octahedral sites.[25] The calculated $Fe1^{3+}/Fe2^{3+}$ ratio of 1/1 indicates that the iron is distributed over two crystallographic sites. This is in good agreement with the crystal structure in which the transition metal atoms are

located at the 8*g* (1/4 0.636 1/4) and the 4*a* (1/2 1/2 1/2) atomic positions (Table 2). This implies the presence of a statistical disorder of Ni^{2+} and Fe^{3+} which leads to the final chemical formula α-$Na_2[Ni1_{3/2}Fe1_{1/2}]$ $[Ni2_{1/2}Fe2_{1/2}](PO_4)_3$. One should mention that in the high temperature form β-$Na_2Ni_2Fe(PO_4)_3$, a perfect ordering of Ni^{2+} and Fe^{3+} has been observed.

3.5. Magnetic properties

The magnetic susceptibility χ vs. T and the corresponding χ^{-1} vs. T for α-$Na_2Ni_2Fe(PO_4)_3$ measured under 100 Oe and associated with zero-field-cooling magnetization (M_{ZFC}) is shown in Fig. 6. The χ^{-1} vs. T plot reveals that α-$Na_2Ni_2Fe(PO_4)_3$ exhibits a paramagnetic behavior in the temperature range 100 – 350 K. The susceptibility above 100 K follows a Curie-Weiss law with θ = –114.3 K. The negative θ indicates that the predominant spin exchange interactions are antiferromagnetic (AFM). The effective magnetic moment μ_{eff} calculated from the Curie constant 7.14 μ_B is in agreement with the effective moment of 7.01μ_B expected for one high-spin Fe^{3+} (S = 5/2), and two Ni^{2+} (S = 1) atoms.

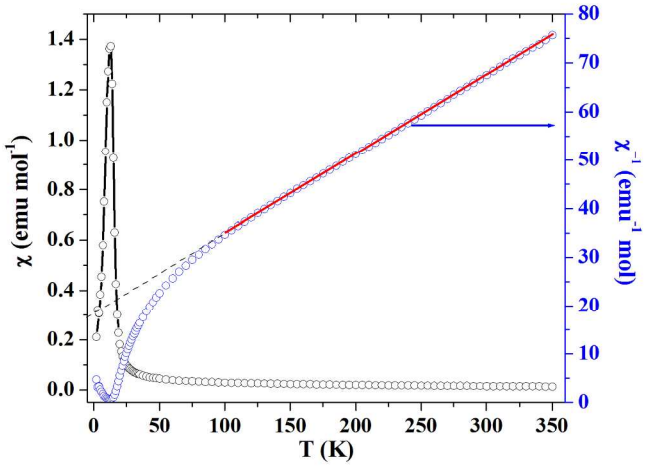

Fig. 6. Magnetic susceptibility χ vs. Temperature and the corresponding χ^{-1} vs. T plots of α-$Na_2Ni_2Fe(PO_4)_3$ measured with the applied field H = 100 Oe.

3.6. Electrochemical properties

3.6.1. α-$Na_2Ni_2Fe(PO_4)_3$ as anode for sodium cells

Fig. 7 shows the initial charge/discharge cycle of a α-$Na_2Ni_2Fe(PO_4)_3$/$NaPF_6$-EC-DMC/Na half-cell, between 0.03 and 3.0 V, at a 50 mA/g current density. The material undergoes an intercalation/conversion reaction in which the first discharge capacity of 960 mAh/g corresponds to the reaction of more than seven sodium atoms. This capacity is much higher than the theoretical value 371 mAh/g expected for the reduction of one Fe^{3+} to Fe^0 and two Ni^{2+} to Ni^0. The origin of the additional contribution is still unclear although one can suspect the reduction of the electrolyte over the material/carbon interface as a possible mechanism.

The first discharge curve, signals an intriguing behaviour corresponding to the appearance of three pseudo-plateaus. The first one, observed between 2.75 and 1 V, corresponds to the reduction of Fe^{3+} to Fe^{2+}, since the obtained discharge capacity of 53.5 mAh/g corresponds to the intercalation of one sodium atom. Such a plateau has been often observed in iron phosphates, such as $NaMnFe_2(PO_4)_3$.[5] The two additional plateaus, observed between 1 and 0.5 V, and between 0.5 and 0.03V, correspond to the $Fe^{2+/0}$, $Ni^{2+/0}$ redox couples, and most probably to the reduction of the electrolyte and/or the formation of oxides at the electrode interface (SEI), respectively. It should be mentioned that the reduction of M^{2+} to M^0 has been already observed in oxyphosphates $M_{0.5}TiOPO_4$ (*M*: Ni, Co and Fe).[26-29] Fig. 8. shows the rate capability of α-$Na_2Ni_2Fe(PO_4)_3$. Under the current rates of 50, 100, 200, and 400 mA/g, reversible capacities of 238, 196, 153, and 115 mAh/g, were obtained, respectively.

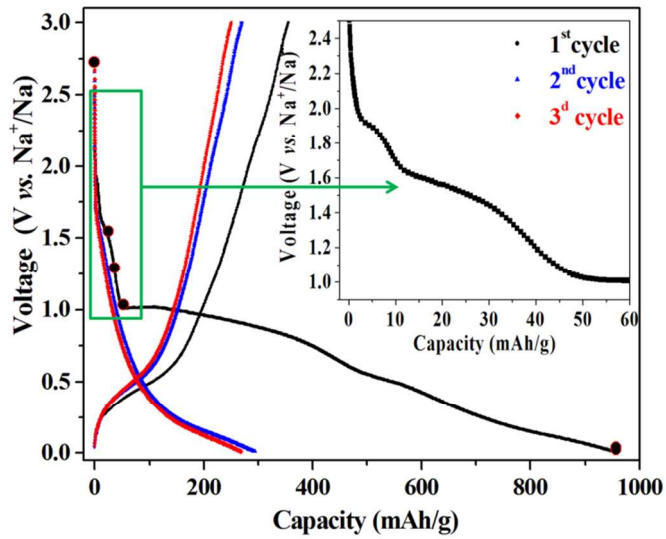

Fig. 7. The charge-discharge curves of α-$Na_2Ni_2Fe(PO_4)_3$ at a current density of 50 mA/g. The inset corresponds to a zoom of the first discharge curve in the capacity area 0 to 60 mAh/g.

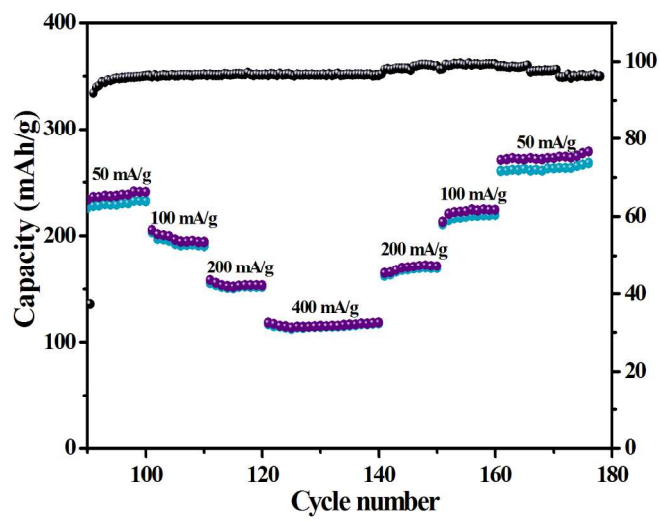

Fig. 8. Performance of α-$Na_2Ni_2Fe(PO_4)_3$ as negative electrode in the voltage range 0.03-3 V *vs.* Na^+/Na, at 20 °C.

3.6.2. α-$Na_2Ni_2Fe(PO_4)_3$ as cathode for sodium cells

As mentioned in section 2.6., upon the intercalation of one sodium atom into α-$Na_2Ni_2Fe(PO_4)_3$ a new phase α-$Na_3Ni_2Fe(PO_4)_3$was formed. The electrochemically as-prepared material was then evaluated as a cathode by a galvanostatic charge/discharge cycling at 5 mA/g current rate in the voltage range 1.8–4.5 V *vs.* Na^+/Na (Fig. 9).

During the first charge, $Na_3Ni_2Fe(PO_4)_3$ delivers a capacity of 160 mAh/g in good agreement with the theoretical capacity

expected from the extraction of three sodium atoms and corresponding to the oxidation of one Fe^{2+} to Fe^{3+} and two Ni^{2+} to Ni^{3+}. During the first discharge, $Na_3Ni_2Fe(PO_4)_3$ delivers a capacity of 92 mAh/g, which is similar to the capacities reported for $Na_2Fe_{3-x}Mn_x(PO_4)_3$(93 mAh/g) and $Na_2Mn_2Fe(PO_4)_3$ (60 mAh/g) crystallizing with the allaudite-type structure.[5, 7] It is worth noticing that the electrochemical activity of $Na_3Ni_2Fe(PO_4)_3$, centred at 3.59 V *vs*. Na^+/Na, is different from the redox potentials observed in $NaFePO_4$ (2.7 V),[8] $Na_2FeP_2O_7$ (3 V),[10] and $Na_4Fe_3(PO_4)_2(P_2O_7)$ (3.2 V),[11] but close to the one observed in $Na_4Ni_3(PO_4)_2(P_2O_7)$ (3.75 V). This confirms that the redox potential is very sensitive to the crystal structure and the coordination of the transition metal atoms.

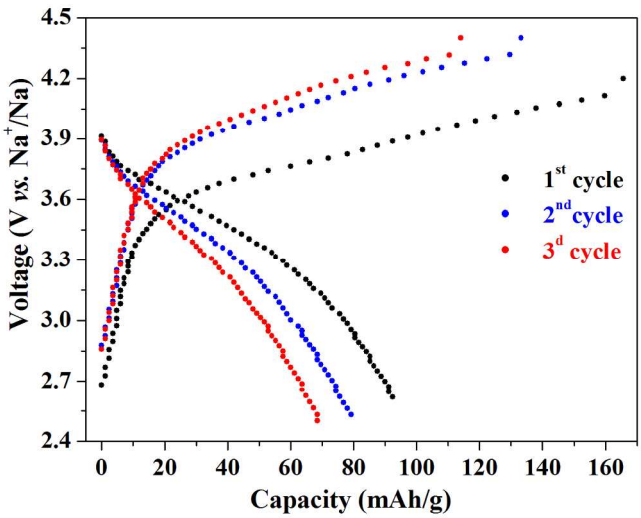

Fig. 9. Galvanostatic charge/discharge profiles of $Na_3Ni_2Fe(PO_4)_3$ in a Na-ion cell at 5 mA/g current rate in the voltage range 1.8–4.5 V

It is also worth mentioning that the PXRD patterns of $Na_3Ni_2Fe(PO_4)_3$ and α-$Na_2Ni_2Fe(PO_4)_3$ are very similar (not shown here). The slight increase of cell parameters of α-$Na_2Ni_2Fe(PO_4)_3$ from a = 10.42821(12), b = 13.19862(15), c = 6.47634(8) Å, and V = 891.39 (2) $Å^3$ to a = 10.46388, b = 13.25538, c = 6.47845 Å, and V = 898.6 $Å^3$ after the intercalation of one sodium atom is expected. The exact atomic position of the intercalated Na atom remains undetermined due to the poor quality of the PXRD pattern. However, the examination of the crystal structure indicates the presence of vacancies at the 4c (1/4, 1/4, 1/4) atomic position, in which one sodium might be intercalated (Fig. S3). Further experiments using synchrotron X-ray diffraction, high resolution electron diffraction (HRTEM), neutron diffraction, and ^{23}Na- and ^{31}P-NMR are being conducted to solve the crystal structure of $Na_3Ni_2Fe(PO_4)_3$, and whose results will be reported elsewhere.

4. Conclusion

The new compound α-$Na_2Ni_2Fe(PO_4)_3$, synthesized by a solid state reaction route, and its structure was determined based on a stuffed α-$CrPO_4$-type structural model. The sodium atoms are located within 3D-framework of octahedra and tetrahedra sharing corners and/or edges with channels along [100] and [010]. The ^{57}Fe Mössbauer spectrum indicates that the Fe^{3+} is distributed over two crystallographic sites with the presence of a Ni^{2+}/Fe^{3+}statistical disorder. The magnetic susceptibility follows the Curie-Weiss behavior above 100 K with θ = -114.3 K indicating predominant antiferromagnetic interactions. The electrochemical tests indicate that during the first discharge to 0.03 V *vs*. Na^+/Na, α-$Na_2Ni_2Fe(PO_4)_3$ delivers a capacity higher than the expected value of 371 mAh/g which corresponds to the reaction of seven sodium atoms. This indicates the presence of a conversion-type behaviour beside a possible reduction of the electrolyte. When α-$Na_2Ni_2Fe(PO_4)_3$ is discharged only to 1 V *vs*. Na^+/Na (53.5 mAh/g), one Na^+ could be intercalated into the structure. The new material $Na_3Ni_2Fe(PO_4)_3$ has demonstrated the potential of use as a cathode with an initial discharge capacity of 90 mAh/g and average voltage around 3.5 V. This dual behaviour anode/cathode of $Na_2Ni_2Fe(PO_4)_3$ can open up new horizons for practical sodium cell chemistries.

Notes and references

[a] Qatar Environment and Energy Research Institute, Qatar Foundation, P.O. Box 5825, Doha, Qatar.
[b] Departamento de Física de la Materia Condensada, Universidad del País Vasco, P.O. Box 644, Bilbao, Spain.
[c] Laboratory of Mineral Solid and Analytical Chemistry "LCSMA", Department of Chemistry, Faculty of Sciences, University Mohamed I, Po. Box 717, 60050 Oujda, Morocco.
[d] Pôle Energies Renouvelables et Etudes Pétrolières, Université Internationale de Rabat, 11000 – Salé el Jadida, Technopolis, Morocco.
[e] Institute of New Energy Material Chemistry, Nankai University, Tianjin 300071, China.

Corresponding authors:
H. Ben Yahia (Hyahia@qf.org.qa)
I. Belharouak (ibelharouak@qf.org.qa)
R. Essehli (ressehli@qf.org.qa)

† Electronic Supplementary Information (ESI) available: See DOI: 10.1039/b000000x/

1 C. Delmas, M. Maccario, L. Croguennec, F. Le Cras, and F. Weill, *Nat. Mater.*, 2008, **7**, 665.
2 S. Franger, F. Le Cras, C. Bourbon, and H. Rouault, *Electrochem. Solid-State Lett.*, 2002, **5**, 231.
3 M. Nose, H. Nakayama, K. Nobuhara, S. Nakanishi, and H. Iba, *J. Power Sources*, 2013, **234** , 175.
4 M. Nose, S. Shiotani, H. Nakayama, K. Nobuhara, S. Nakanishi, and H. Iba, *Electrochem. Commun.*, 2013, **34**, 266.
5 K. Trad, D. Carlier, L. Croguennec, A. Wattiaux, M. Ben Amara, and C. Delmas, *Inorg. Chem.*, 2010, **49**, 10378.
6 K. Trad, D. Carlier, A. Wattiaux, M. Ben Amara, and C. Delmas, *J. Electrochem. Soc.*, 2010, **157**, A947.
7 W. Huang, B. Li, M. F. Saleem, X. Wu, J. Li, J. Lin, D. Xia, W. Chu, and Z. Wu, *Chem. Eur. J.*, 2014, **20**, 1.
8 P. Moreau, D. Guyomard, J. Gaubicher, and F. Boucher, *Chem. Mater.*, 2010, **22**, 4126.
9 W. Huang, J. Zhou, B. Li, J. Ma, S. Tao, D. Xia, W. Chu, and Z. Wu, *Scientific Reports*, 2014, 4: 4188, DOI: 10.1038/srep04188.
10 P. Barpanda, T. Ye, S. Nishimura, S. C. Chung, Y. Yamada, M. Okubo, H. S. Zhou and A. Yamada, *Electrochem.Commun.*, 2012, **24**, 116.

11 H. Kim, I. Park, D. H. Seo, S. Lee, S. W. Kim, W. J. Kwon,Y. U. Park, C. S. Kim, S. Jeon, and K. Kang, *J. Am. Chem. Soc*., 2012, **134**, 10369.
12 W Song, X Ji, Z Wu, Y Zhu, Y Yao, K Huangfu, Q Chen and C. E. Banks, *J. Mater. Chem. A*, 2014, **2**, 2571.
13 F. Hatert, P. Keller, F. Lissner, D. Antenucci, and A. M. Fransolet, *Eur. J. Mineral*., 2000, **12**, 847.
14 R. Essehli, B. El Bali, S. Ben Mokhtar, K. Bouziane, B. Manoun, M. A. Abdalslam, and H. Ehrenberg, *J. Alloys Compd*., 2011, **509**, 1163.
15 V.Petricek, M. Dusek, and L. Palatinus, *Z. Kristallogr*., (2014). **229(5)**, 345.
16 N.Kinomura, N., Matsui, N. Kumada, and F. Muto, *J. Solid State Chem*.,1989, **79**, 232.
17 P.-E. Werner, L. Eriksson, and M. Westdahl, TREOR, a Semi-Exhaustive Trial-and-Error Powder Indexing Program for All Symmetries, *J. Appl. Cryst*., 1985, **18**, 367.
18 A. Boultif and D. Louër, *J. Appl. Crystallogr*.,1991, 24, 987.
19 M. B. Korenski, J. W. Kolis, and G. J. Long, *J. Solid State Chem*., 1999, **147**, 390.
20 J.P. Attfield, P.D. Battle, and A.K. Cheetham, *Nature*,1986, **322**, 620.
21 I. D. Brown and D. Altermatt, *Acta Crystallogr*., 1985, **B41**, 244.
22 N. E. Brese and M. O'Keefe, Acta Crystallogr., 1991, **B47**, 192.
23 R. Perret and A. Boudjada, *C. R. Seances Acad. Sci*.,1979, **Ser. C**, 288.
24 R. D. Shannon, *Acta Crystallogr*., 1976, **A32**, 751.
25 K. Trad, D. Carlier, L. Croguennec, A. Wattiaux, M. Ben Amara, and C. Delmas, *Inorg. Chem*., 2010, **49**, 10378.
26) I. Belharouak and K. Amine, *Electrochem. Commun*., 2005, **7**, 648.
27) R. Essehli, B. El Bali, A. Faik, S. Benmokhtar, B. Manoun, Y. Zhang, X.J. Zhang, Z. Zhou and H. Fuess, *J. Alloys Compd*., 2012, **530(0)**, 178.
28) K. Lasri, I. Saadoune, Y. Bentaleb, D. Mikhailova, H. Ehrenberg, L. Häggström and K. Edström, *Solid State Ionics*, 2012, 224,15.
29) R. Essehli, B. El Bali, A. Faik, M. Naji, S. Benmokhtar, Y.R. Zhong, L.W. Su, Z. Zhou, J. Kim, K. Kang and M. Dusek,. *J. Alloys Compd*., 2014, **585(0)**, 434.